NOVOSIBIRSK STATE UNIVERSITY

International Summer School

NONLINEAR PHOTONICS

21–24 AUGUST 2018

Proceedings

Novosibirsk
2018

УДК 535.92
ББК В343.131я431
Н492

Н492 Нелинейная фотоника : Материалы Междунар. школы для молодых ученых (Workshop and Summer school on Nonlinear Photonics) / Новосиб. гос. ун-т. – Новосибирск: ИПЦ НГУ, 2018. – 32 с.

Nonlinear Photonics : Proceedings of Workshop and Summer school / Novosibirsk State University. – Novosibirsk, Russian Federation, 2018. – 32 p.

ISBN 978-5-4437-0807-2

The school brings together the world's leading experts in the field of nonlinear photonics and emerging photonic technologies to share with young researchers their knowledge and interdisciplinary approaches for understanding and designing complex photonic systems. The school will cover a broad spectrum of problems in different aspects of nonlinear photonics from the fundamental science to practical applications. The school will be structured around comprehensive review talks from major world leading experts in complementary areas of nonlinear photonics both on theory, experiment and applications.

УДК 535.92
ББК В343.131я431

ISBN 978-5-4437-0807-2

Whispering Gallery Mode Resonator Introduced on the Surface of Bent Optical Fiber

D.V. Bochek[1*], I.D. Vatnik[1], D.V. Churkin[1], M.Y. Sumetsky[2]
[1]Novosibirsk State University, Novosibirsk, Russia
[2]Photonics Research Group, School of Engineering and Applied Science, Aston University, Birmingham, UK
**d.bochek@g.nsu.ru*

Surface Nanoscale Axial Photonics (SNAP) is a photonic platform for fabrication of miniature optical structures at the optical fiber surface with ultrahigh precision and ultralow losses [1]. In SNAP structures, whispering gallery modes (WGMs) circulate circumferentially around the surface of an optical fiber while undergoing slow propagation along the fiber axis. The WGM propagation is fully controlled by the introduced nanoscale effective radius variation (ERV) of the optical fiber, which includes the contribution from the variation of refractive index and physical dimensions of the fiber. The propagation is readily described by the one-dimensional Schrödinger equation. SNAP devices can be manufactured with unprecedented sub-angstrom precision [2] using simple techniques of controlled local heating with CO2 laser radiation [1] and by the femtosecond laser inscription [3]. High fabrication precision of SNAP devices and their ultralow losses allow one to create complex miniature photonic circuits having promising applications in communication technologies, quantum computing, microfluidics, and sensing.

In the paper we introduce a new method of fabrication of Surface Nanoscale Axial Photonics (SNAP) structures. We show experimentally that a SNAP microresonator with nanoscale effective radius variation can be introduced by bending of an optical fiber. Our approach is much simpler than those developed previously and consists in controllable fiber bending. We showed numerically and experimentally that the bent fiber can achieve the nanometer-scale variation in the effective fiber radius caused by the introduced physical deformation and elasto-optic effect. Due to the positive sign of the ERV, this local bending introduces a SNAP optical bottle resonator [1] which can be tuned by advanced mechanical manipulations of fiber ends. In addition, the proposed method can be applied for tuning of SNAP structures which are fabricated by the methods developed previously. Our results are in reasonable agreement with the developed theory.

We determined the ERV introduced by bending of the standard SMF-28 optical fiber by numerical modelling using COMSOL. Our numerical results show that bending of the silica fiber with realistic bending radius R can cause the increase of the effective fiber radius by several nanometers, which is sufficient to introduce SNAP resonators. For example, bending of SMF-28 125 μm diameter silica fiber with curvature radius 1 cm introduces the positive ERV equal to 4 nm.

To determine the ERV of bent optical fiber experimentally we measured WGMs spectra along the fiber axis. Fiber was fixed in a narrow tube, thereby acquiring the shape of a loop. In such configuration, the fiber curvature has a smooth distribution with a maximum at the center of the loop. WGMs were excited in an optical fiber using a microfiber (MF) [4], specifically, a micrometer diameter waist of a biconical fiber taper, which was attached transversely to the loop and connected to the light source and detector. We measured the spectra along length of the loop in steps of 250 μm. The surface plot of transmission spectra of the resonator introduced by bending of the fiber is shown in Fig. 1.

The introduced ERV Δr is determined from the resonant wavelength variation $\Delta\lambda$ by the rescaling relation $\Delta\lambda = \lambda_0 \cdot \Delta r_{eff} / r_0$ where the wavelength λ_0 = 1552 nm and r_0 = 62.5 μm. From this relation, the maximum wavelength variation $\Delta\lambda$ = 0.3 nm corresponds to the ERV Δr = 12.1 nm.

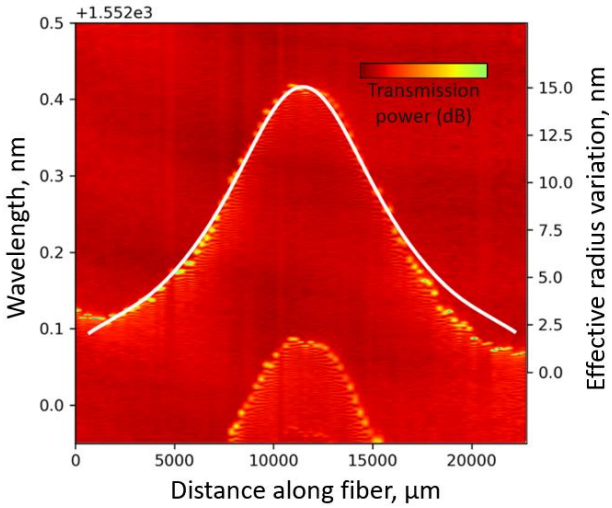

Fig. 1. Experimental characterization of the nanoscale effective radius variation and spectra of the fabricated SNAP structure introduced by bending of optical fiber. White line is the rescaled curvature of the fiber loop

We have demonstrated the possibility to fabricate SNAP microresonators by bending the optical fiber. In our first proof of concept experiment, a simplest optical bottle resonator with ERV of ~ 10 nm was fabricated by bending a commercial 125 μm diameter optical fiber. SNAP structures with more complex shapes can be fabricated by advanced bending techniques using specially prepared fiber bending setups. Our simulation results are in reasonable agreement with experimental observations. The simplicity of the developed method and the ability to tune the introduced resonant structures mechanically is of great importance for the creation of robust and tunable SNAP devices for applications in optical signal processing and ultraprecise sensing.

This work is supported by Russian Science Foundation, №18-72-10053.

References

[1] M. Sumetsky, "Nanophotonics of optical fibers," Nanophotonics **2**, 393 (2013).

[2] N. A. Toropov, and M. Sumetsky, "Permanent matching of coupled optical bottle resonators with better than 0.16 GHz precision," Opt. Lett. **41**, 2278 (2016).

[3] F. Shen, X. Shu, L. Zhang, and M. Sumetsky, "Fabrication of surface nanoscale axial photonics structures with a femtosecond laser," Opt. Lett. **41**, 2795 (2016).

[4] J. C. Knight, G. Cheung, F. Jacques, and T. A. Birks, "Phase-matched excitation of whispering-gallery-mode resonances by a fiber taper," Opt. Lett. 22(15), 1129–1131 (1997).

Influence of Structural Motif on Crystals Functional Properties

A.A. Goloshumova[1,2], L.I. Isaenko[1,2], K.E. Korzhneva[1,2], A.Yu. Tarasova[1,2], A.P. Yelisseyev[1,2], P.G. Krinitsin[1,2]

[1]V.S. Sobolev Institute of Geology and Mineralogy of Siberian Branch of Russian Academy of Sciences, Novosibirsk, Russia

[2]Novosibirsk State University, Novosibirsk, Russia

**goloshumova@igm.nsc.ru*

Nonlinear crystalline materials are extremely demanded for laser radiation conversion. Wide variety of different tasks require big diversity of such properties as transparency, optical stability and many others. It is a well-known fact that a composition and a structure determine the functional properties of crystalline nonlinear materials. Therefore, the goal of the present work was to determine the changes in functional properties and to find the optimal compositions for 2 groups of nonlinear crystals: Li-containing chalcogenides and double nitrates. The first group includes crystals of $LiBC_2$ family (B = In, Ga; C = S, Se, Te) that are effective materials for laser radiation conversion in mid IR region [1-5]. Multicomponent nitrates are promising for using in short wavelength region but still poorly investigated.

Chalcogenide crystals were grown by the vertical Bridgman method, double nitrate crystals were obtained from water solutions. To characterize studied materials a set of methods including X-Ray powder and single crystal analyses, differential thermal analysis, transmission spectra measurements, luminescence spectroscopy etc. were used.

For $LiBC_2$ family it was found that the Ga → In substitution and anion change in S → Se → Te raw lead to the nonlinear coefficient increasing. Sulfide and selenide crystals have orthorhombic symmetry (mm2), while tellurides have tetrahedral structures (-42m). Because of the difference in connection of cation tetrahedra with empty polyhedra in orthorhombic and tetrahedral structures, a higher cation mobility and a larger amount of point defects are more probable in tellurides, and it is these crystals that have higher nonlinear efficiency. It was also revealed that about 10% of Li^+ ions can shift from tetrahedral positions to octahedral ones in $LiInSe_2$ crystal structure. The same situation was observed in mixed $LiGa_{0.5}In_{0.5}Se_2$ crystals. The addition of another compound impacts the properties of $LiBC_2$ crystals. Authors showed that there is higher nonlinear susceptibility and a reduction of band gap values in Li/Ga/Ge/(S,Se) crystals compared to respective double chalcogenides.

In spite of the interest to double nitrates there were contradictory literature data of their physical properties and crystal structures up to now. $K_2Ba(NO_3)_4$, $Pb_{1-x}Ba_x(NO_3)_2$ bulk crystals of an optical quality were grown. Their crystal structures were defined reliably as I-42m and Pa-3, respectively. $Pb_{0.75}Ba_{0.25}(NO_3)_2$, $Pb_{0.68}Ba_{0.32}(NO_3)_2$, $Ba_{0.58}Pb_{0.42}(NO_3)_2$, $Ba_{0.73}Pb_{0.27}(NO_3)_2$ crystals were obtained for the first time. It was proved that $Pb_{1-x}Ba_x(NO_3)_2$ is a solid solution, where Pb/Ba^{2+} cations share the same crystallographic position. Crystal structure is close to the one of simple Ba-nitrate with the unit cell parameters decreasing linearly with the increase of Pb content. In $K_2Ba(NO_3)_4$ cations of different charge each have their independent position in crystal structure, triangles of NO_3 group are distorted. These crystals were shown to possess nonlinear properties and may be regarded as promising materials for short wavelength region.

The present work was supported by the Russian Foundation for Basic Research (grants №№ 18-32-00359, 17-45-540775).

References

[1] L. Isaenko, A. Yelisseyev, S. Lobanov, A. Titov, V. Petrov, J.-J. Zondy, P. Krinitsin, A. Merkulov, V. Vedenyapin, J. Smirnova, "Growth and properties of $LiGaX_2$ (X = S, Se, Te) single crystals for nonlinear optical applications in the mid-IR," Cryst. Res. Technol. **38**, 379 (2003).

[2] Isaenko L., Yelisseyev A., Lobanov S., Krinitsin P., Petrov V., Zondy J-J., "Ternary chalcogenides $LiBC_2$ (B=In,Ga; C=S,Se,Te) for mid-IR nonlinear optics," J. Non-Cryst. Sol. **352**, 2439 (2006).

[3] Yelisseyev A. P, Titov A. S, Isaenko L. I, Lobanov S. I, Lyapunov K. M, Gruzdev V. A, Komarov S. G, Drebushchak V. A, Petrov V., Zondy J-J., "Thermal properties of the midinfrared nonlinear crystal $LiInSe_2$," J. Appl. Phys. **96**, 3659 (2004).

[4] Takeya K., Takemoto Y., Kawayama I., Murukami H., Marsukawa T., Yoshimura M., Mori Y., Tonouchi M., "Terahertz Generation and Optical Properties of Lithium Ternary Chalcogenide Crystals," J. Infrared Millim. THz Waves. **32**, 426 (2011).

[5] L.I. Isaenko, A.P. Yelisseyev. "Recent study of nonlinear crystals for the mid IR," Semicond. Sci. Tech. **31**, 123001 (2016).

Supercontinuum Generation in the Monocrystalline Optical Fibers

V.A. Kamynin[1*], A.I. Trikshev[1], S.A. Filatova[1], I.V. Zhluktova[1], S.Y. Rusanov[1], V.B. Tsvetkov[1,2]

[1]Prokhorov General Physics Institute of Russian Academy of Sciences, Moscow, Russia

[2]National Research Nuclear University, "MEPhI", Moscow, Russia

* kamyninva@gmail.com

Supercontinuum (SC) sources find more and more fields of an application at present moment. Today one can find such sources in high-speed telecommunication systems [1], terahertz systems and etc. As basic elements of SC generators usually are used high-power short-pulse lasers and nonlinear media. To achieve short pulse generation, one uses semiconductor saturable absorber mirrors (SESAMs), saturable absorbers based on single-wall carbon nanotubes, nonlinear fiber mirrors, and nonlinear polarization ellipse rotation. To obtain high power one can use simple amplification (one or few fiber amplifiers) or OPCPA system. At present moment as the nonlinear medium for SC generation were used standard telecommunication fibers, germanium-doped fibers, different types of waveguides, ZBLAN fibers and etc. One of the promising material for SC generation is a single crystal or monocrystalline fiber (MCF) [2, 3].

In our work, we have investigated SC generation in the two MCFs. One was 800 um diameter and 110 mm length, another was 520 um diameter and 90 mm length. Both specimens were made of sapphire. As the pump source home-made all-fiber holmium laser was used. To increase peak power of the 1.7 ps pulses holmium-doped fiber amplifier was used. 1.2 m germanium-doped fiber was added to the scheme for spectral pre-broadening.

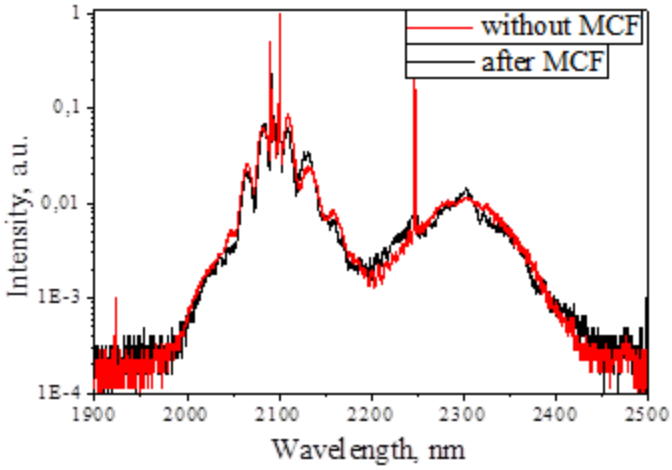

Fig. 1. Output spectra of SC generation without MCF (red curve) and after MCF (black curve)

The output spectra of SC generation without MCF (red curve) and after MCF (black curve) are shown at the figure 1. As one can see SC spectrum that produced after MCF had longer spectral generation. So MCF can be used for SC generation, but, as we suppose, more peak power is required.

References

[1] H. Hu et al. "Single-source chip-based frequency comb enabling extreme parallel data transmission," Nature Photonics **12**, 469 (2018).

[2] W. M. Nakaema et al. "Supercontinuum generation in a sapphire fiber and comparison with a compact PCF based light source," Quantum Electronics and Laser Science Conference, p. JThB97 (2011).

[3] J. H. Kim et al. "Broadband IR supercontinuum generation using single crystal sapphire fibers," Optics express **16**, 4085 (2008).

Bismuth-Doped Fiber Lasers Mode-Locked by Nonlinear Loop Mirror

A.M. Khegai[1,2*], M.A. Melkumov[1], K.E. Riumkin[1], E.M. Dianov[1]
[1]Fiber Optics Research Center of the Russian Academy of Sciences, Moscow, Russia
[2]A.M. Prokhorov General Physics Institute of the Russian Academy of Sciences, Moscow, Russia
*khegai@fo.gpi.ru

The bismuth fiber is a new laser media actively investigated in recent decades. In a short period of time from the beginning of the 2000s to the present day, numerous of efficient and powerful sources and amplifiers based on bismuth fibers operating in a wide spectral range from 1100 nm to 1800 nm have been demonstrated. In this paper, we describe bismuth-doped fiber lasers mode-locked by nonlinear loop mirror, operating at about 1.3 and 1.7 μm. Pulsed lasers generating at the stated spectral regions are of great importance for research and application. In particular, radiation in the region of 1.3 and 1.7 μm is interesting for biophotonics due to the fact that these spectral bands correspond to the transparency windows of biological tissues [1,2].

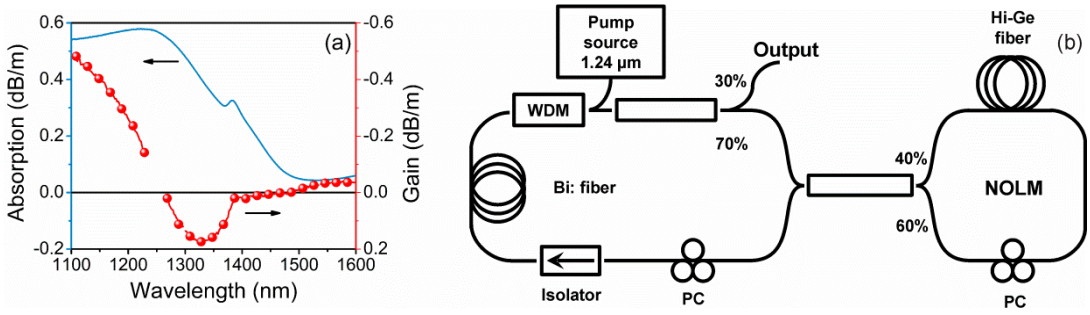

Fig. 1. Absorption and gain spectra of phosphosilicate fiber doped with bismuth (a). Schematic of the pulsed laser at 1.3 μm based on NOLM (b)

To obtain optical gain in the regions of 1.3 and 1.7 μm, we used phosphorosilicate and germanosilicate (50 mol. % GeO_2) bismuth fibers, respectively. Characteristic absorption and gain spectra in such fibers are shown in Fig. 1 (a) and Fig. 2 (a).

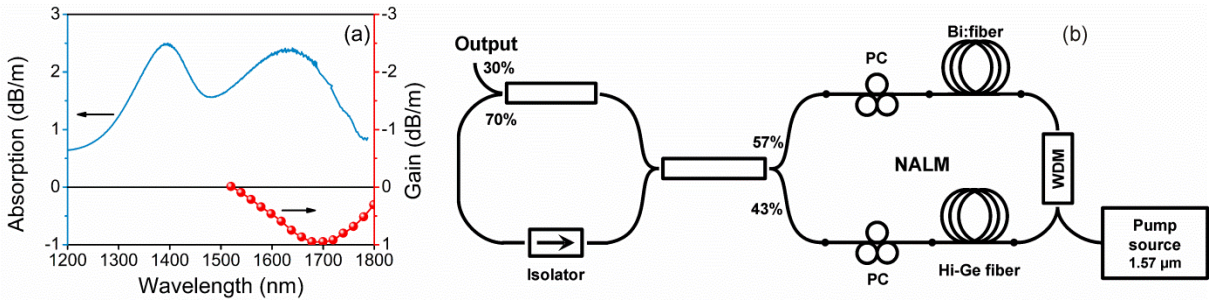

Fig. 2. Absorption and gain spectra of high-germanium fibers doped with bismuth (a). Schematic of pulsed laser at 1.7 μm based on NALM (b)

The cavities of the lasers was based on classic figure-of-eight scheme with nonlinear optical loop mirror (NOLM) in case of the oscillator at 1.3 μm (see Fig. 1(b)) and nonlinear amplifying loop mirror (NALM) for the source at 1.7 μm (see Fig. 2(b)). For efficient operation of the nonlinear mirror as a mode-locker, the segment of a passive high-germanium (30 mol. % GeO_2) fiber having a high nonlinearity as compared with a standard SMF-28 fiber was added in the Sagnac loop. Additionally, in both cases an optical isolator and a pair of polarization controllers (PCs) were

incorporated into the cavity, the first one to provide unidirectional operation outside the loop mirror and the second one to adjust the polarization state of the radiation inside the laser.

In the described schemes, generation of picosecond pulses was obtained. To start-up the passive mode-locking the precise PCs adjustment as well as external intervention (e.g., bending of short peace of the fiber or tapping the fiber spool) was required. In the case of a phosphosilicate fiber laser, the shape of the spectrum had steep edges and a flat top, specific to dissipative solitons (see Fig. 3(a)), while the shape of the spectrum for the oscillator on the high-germanium fiber was close to the parabola that could point out the generation of similaritons (see Fig. 3(b)) [3]. The output characteristics of lasers are presented in Table 1.

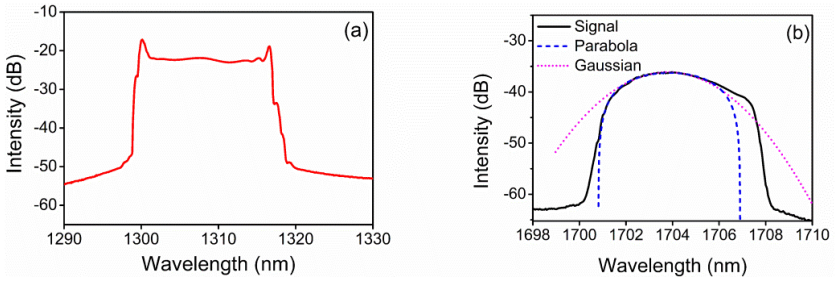

Fig. 3. Spectrum of the pulsed lasing at 1.3 μm (a) and 1.7 μm (b)

Table 1. Output parameters of the lasers at 1.3 and 1.7 μm

Parameters of the pulsed regime	Laser type	
	Laser at 1.3 μm	Laser at 1.7 μm
Pulse duration (FWHM), ps	11.3	17.7
Energy, nJ	1.6	0.084
Repetition rate, MHz	3.5	3.57

In summary, the passive mode-locking in the figure-of-eight laser schemes based on phosphosilicate and high-germanium fibers doped with bismuth, operating at 1.3 and 1.7 μm was demonstrated.

The work was supported by Russian Science Foundation (RSF) (16-19-10688).

References

[1] D. Kobat, M. E. Durst, N. Nishimura, A. W. Wong, C. B. Schaffer, and C. Xu, "Deep tissue multiphoton microscopy using longer wavelength excitation," Opt. Express **17**, 13354 (2009).

[2] N. G. Horton, K. Wang, D. Kobat, C. G. Clark, F. W. Wise, C. B. Schaffer, and C. Xu, "In vivo three-photon microscopy of subcortical structures within an intact mouse brain," Nat. Photonics **7**, 205 (2013).

[3] W. H. Renninger, A. Chong, and F. W. Wise, "Pulse shaping and evolution in normal-dispersion mode-locked fiber lasers," IEEE J. Sel. Top. Quantum Electron. **18**, 389 (2012).

All Fiber Combined Er/Er-Yb Fiber Amplifier

M.M. Khudyakov[1,2*], A.S. Lobanov[3], D.S. Lipatov[3], N.N. Vechkanov[3], A.N. Gur'yanov[3], M.M. Bubnov[1], M.E. Likhachev[1]

[1]Fiber Optics Research Center of the Russian Academy of Sciences, Moscow, Russia
[2]Moscow Institute of Physics and Technology (State University), Moscow, Russia
[3]Institute of Chemistry of High-Purity Substances, Russian Academy of Sciences, Nizhnii Novgorod, Russia
**DAngeL.74@gmail.com*

Laser sources operating in the spectral range near 1.55 μm are widely used in telecommunications, atmospheric and space communications and atmospheric sensing. Large mode area (LMA) Er-Yb clad pumped fiber amplifiers are most suited for such tasks having high average output power (111 W) combined with high differential pump-to-signal conversion efficiency (PCE) (46%) and relatively small fiber length (5.5 m) [1]. However, such amplifiers need high input power (2 W) to achieve high PCE. Reduction of input power down to 50 mW results in decrease of PCE down to 5% [2]. Total gain in the both cases is relatively small – 14-17 dB, which is not optimal, as in this case nonlinearity in preamplifier limits maximum achievable peak power. On the contrary Yb-free Er-doped fibers can demonstrate very high gain of more than 30 dB in C-band , but the total efficiency in this case is small (~8-10%) due to a large amount of unabsorbed pump power [3]. In this work to improve total amplification while keeping high PCE we propose to use a combined amplifier based on piece of Er-doped LMA fiber as preamplifier stage directly spliced with Er-Yb LMA fiber to form an all fiber combined amplifier.

Er-doped (Yb-free) fiber used in the current study was similar to one, described in [3]. The fiber has square shaped outer cladding with dimensions of 110x110 μm. Core has diameter of 38 μm and was doped with 0.1 mol.% of Er_2O_3 in P_2O_5-Al_2O_3-SiO_2 glass matrix. Fundamental mode field diameter (MFD) was estimated to be 26.7 μm.

The Er-Yb fiber was based on newly developed phosphorosilicate glass matrix highly doped with fluorine [4] containing 0.001 wt.% of Er_2O_3 and 0.9 wt.% of Yb_2O_3. It has square shaped outer cladding with dimensions of 145x145 μm, core diameter of 25.6 μm and calculated MFD of 21.8 μm. Refractive index profiles of both fibers and facet photos are presented at Fig. 1 a)-c).

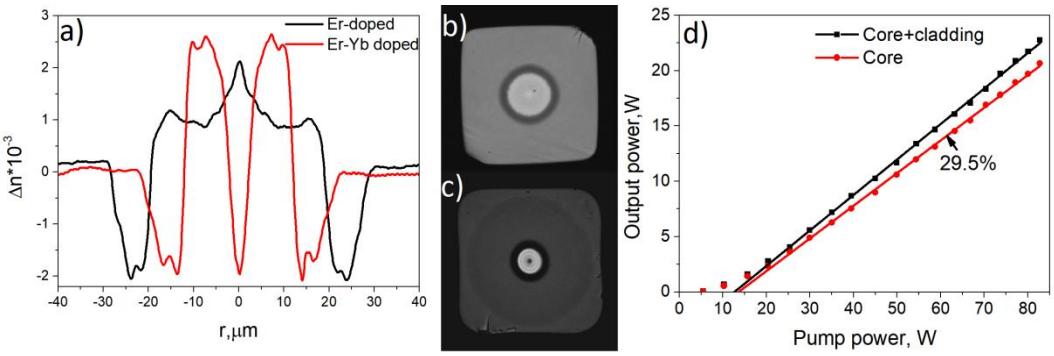

Fig. 1. a)refractive index profile of both fibers; b)facet photo of Er-doped fiber; c)facet photo of Er-Yb doped fiber; d)output power at 1555 nm contained in the core and in both core and cladding versus pump power

The amplifier consisted of 3 meters of Er-doped fiber directly spliced with 5 meters of Er-Yb fiber. The end fiber facet was angle cleaved to prevent reflection. The amplifier was pumped through (2+1) to 1 pump combiner by two 45 W multimode wavelength stabilized at 976 nm laser diode modules. We used radiation of distributed feedback laser diode with central wavelength of 1555 nm amplified by 8/125 μm core pumped Er-doped fiber amplifier up to 50 mW as a seed

source. Results of amplification are presented at Fig. 1d). Due to slight MFD mismatch between Er- and Er-Yb doped fibers up to 1.5 W of output power were propagating outside the core. Total output power at 1555 nm of slightly over 20.5 W was demonstrated with PCE of 29.5 %. Reduction of input signal down to 8 mW didn't reduce output power within accuracy of measurements. , therefore we demonstrated almost and order of magnitude higher total amplification of 26.1 dB compared to [1].

The study was supported by the Russian Science Foundation (RSF) (grant №18-19-00687). The Er-Yb fiber was developed in the frame of grant №17-13-01343 from the Russian Science Foundation (RSF)

References

[1] O. De Varona, W. Fittkau, P. Booker, T. Theeg, M. Steinke, D. Kracht, J. Neumann, and P. Wessels, "Single-frequency fiber amplifier at 15 μm with 100 W in the linearly-polarized TEM_00 mode for next-generation gravitational wave detectors," Opt. Express, **25**, 24880, (2017).

[2] Z. Zhao, H. Xuan, H. Igarashi, S. Ito, K. Kakizaki, and Y. Kobayashi, "Single frequency, 5 ns, 200 μJ, 1553 nm fiber laser using silica based Er-doped fiber," Opt. Express, **23**, 29764, (2015).

[3] L. V Kotov, M. Y. Koptev, E. A. Anashkina, S. V Muravyev, A. V Andrianov, M. M. Bubnov, A. D. Ignat'ev, D. S. Lipatov, A. N. Gur'yanov, M. E. Likhachev, and A. V Kim, "Submicrojoule femtosecond erbium-doped fibre laser for the generation of dispersive waves at submicron wavelengths," Quantum Electron., **44**, 458, (2014).

[4] M. M. Khudyakov, S. S. Aleshkina, T. A. Kochergina, K. K. Bobkov, A. S. Lobanov, D. S. Lipatov, A. N. Abramov, A. N. Gur'yanov, M. M. Bubnov, and M. E. Likhachev, "Single-mode Er- Yb fiber amplifier with large mode area," accepted for publication in Russian Fiber Lasers, Novosibirsk, Russia, 3-7 September, 2018.

Generation of Complex Optical Signals for Data Transmission Systems

L.A. Kochkurov[1*], M.I. Balakin[1], L.A. Melnikov[1], V.O. Anashkina[1], A. Chipouline[2]
[1]Department of Instrumentation Engineering, Yuri Gagarin State Technical University of Saratov, Saratov, Russia
[2]Institute for Microwave Engineering and Photonics, Technische Universität Darmstadt, Merckstr. 25, 64283 Darmstadt, Germany
**lkochkurov@gmail.com*

At the current stage of the development of telecommunications networks one of the main tasks are to increase the data transfer rate. Development of the technology of spectral multiplexing (WDM, DWDM, NyquistWDM) allowed to transfer data with speeds up to 400 Gbit/s [1]. Such speeds are possible only with the use of new modulation formats that use switching of the radiation polarization and phase manipulation of the signal. Widely tunable MEMS (Micro-Electro-Mechanical System) VCSEL, gives the opportunity to change the wavelength of the laser by 100 nm in the region of 1550 nm [2]. Thus, the appearance of tunable VCSEL makes it urgent to study the question of their use in the transmission of optical information using modern transmission formats. Injection locking of semiconductor lasers by external laser with phase manipulated field give regimes with reduced amplitude effects [3].

Here we present a theoretical model of the master-slave injection locked semiconductor laser. Our goal is to specify the operating regimes for previously presented experimental results. The conventional Lang-Kobayashi rate equation [3] for the complex electric field $E(t)$ and carrier number $N(t)$ have often been successfuly used to explain the dynamical behaviour of this type of laser coupling

$$\frac{dE_1(t)}{dt} = (1 - \imath\alpha)\left(G(t) - \frac{1}{\tau}\right)\frac{E_1(t)}{2} + \frac{k_1}{\tau}E_{m1}(t), \quad (1)$$

$$\frac{dE_2(t)}{dt} = (1 - \imath\alpha)\left(G(t) - \frac{1}{\tau}\right)\frac{E_2(t)}{2} + \frac{k_2}{\tau}E_{m2}(t), \quad (2)$$

$$\frac{dN}{dt} = \frac{I}{e} - \frac{N(t)}{\tau_n} - G(t)(|E_1(t)|^2 + |E_2(t)|^2), \quad (3)$$

$$G(t) = \frac{g\,(N(t) - N_0)}{1 + s(|E_1(t)|^2 + |E_2(t)|^2)}, \quad (4)$$

where k represents the portion of the master laser amplitude, that is injected into the slave laser; indexes 1 and 2 corresponts to the first and the second modes; $E_{m1}(t)$, $E_{m2}(t)$ are the injection-locking signals from two different sources. The injected complex field of the master laser is represented by the square wave function in the form $E_m=A(t)\exp[i(\Delta\omega t+\varphi(t))]$, where $\Delta\omega=\omega_m-\omega_s$ is a frequency detuning between master (m) and slave (s) lasers; $A(t)$ and $\varphi(t)$ are the square wave functions describing the amplitude and phase modulation of the master laser signal which we use to simulate the binominal data with 1Gbit/s rate. Such system can demonstrate only two types of behaviours. If $|\Delta\omega/A_m|\leq 1$, all solutions tend to a phase-locked state (filled area on fig.1a), where the slave oscillator maintains a constant phase difference relative to the master (phase-locking or synchronization). In case $|\Delta\omega/A_m|>1$ all solutions exhibit phase drift (unfilled area on fig.1a), where the phase difference grows monotonically, with one oscillator periodically overtaking the other (phase drift or rhythm splitting).

Numerical analysis shows, that smooth variation of the frequency detuning $\Delta\omega$ (Fig.1b) allows each of the generated modes to be tuned to the desired value of the phase difference $\Delta\psi(t)=\psi_s-\psi_m$, where ψ is the "pure" phase of the field. It follows that the phase content of the injected signal is

entirely reproduced by the slave laser (Fig.1c). By injecting an optical field inside a laser cavity, a coupling between phase and field of the interacting waves is taking place leading to an excitation of relaxation oscillations of the injection locked laser. The relaxation process takes about 0.1 ns.

The preceding analysis showed that the considered injection-locked laser is suitable for the replication of encoded signals.

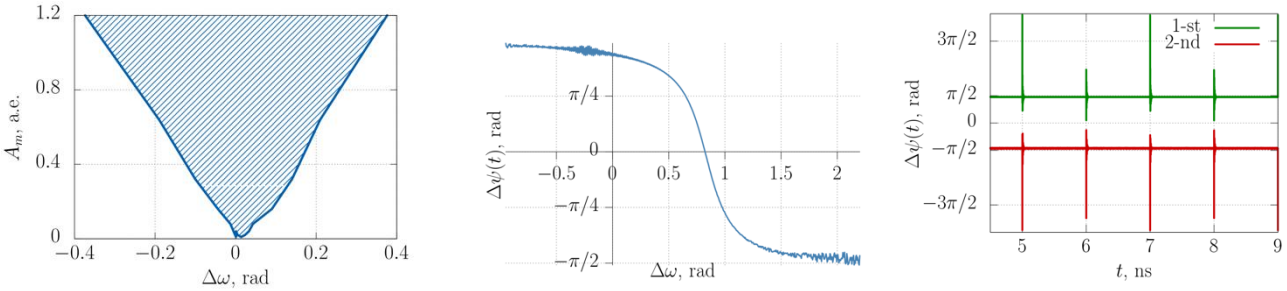

(a) (b) (c)

Fig. 1. (a) - Stability map of an injected semiconductor laser; (b) - phase difference between master and slave lasers as a function of frequency detuning; (c) - phase difference between master and slave laser for the 1st (green) and the 2nd (red) modes as a function of time

This work was financially supported by Russian Foundation for Basic Research (Projects No. 18-08-00599 A, № 18-32-01028); DAAD together with Ministry of Education and Science of the Russian Federation ("Mikhail Lomonosov" Programme -2018).

References

[1] X. Liu, H. Hu, S. Chandrasekhar, R. M. Jopson, A. H. Gnauck, M. Dinu, C. Xie, and P. J. Winzer, "Generation of 1.024-Tb/s Nyquist-WDM phase-conjugated twin vector waves by a polarization-insensitive optical parametric amplifier for fiber-nonlinearity-tolerant transmission," Opt. Express **22**, 6478 (2014).

[2] C. Gierl, T. Gruendl, P. Debernardi, K. Zogal, C. Grasse, H. A. Davani, G. Böhm, S. Jatta, F. Küppers, P. Meißner, and M.-C. Amann, "Surface micromachined tunable 1.55 μm-VCSEL with 102 nm continuous single-mode tuning," Opt. Express **19**, 17336 (2011).

[3] Lang, R., "Injection locking properties of a semiconductor laser," IEEE Journal of Quantum Electronics **18**, 976 (1982).

Self-Adjusting Fibre Mode-Locked Laser with Controllable Nonlinear Phase Shift inside Laser Cavity

***A. Kokhanovskiy*[1*], *A. Ivanenko*[1], *S. Kobtsev*[1], *S. Turitsyn* [1,2]**
[1]*Novosibirsk State University, Novosibirsk, Russia*
[2]*Aston Institute of Photonic Technologies, Aston University, B4 7ET, Birmingham, UK*
**alexey.kokhanovskiy@gmail.com*

Fiber lasers with nonlinear amplifying loop mirrors are widely used to generate stable ultrashort pulses [1] with a relatively high power [2]. The classical scheme of a figure-8 fiber laser resonator with one amplification region has only one degree of freedom-the power of the pump diode, which significantly reduces the variability of the parameters of the pulsed radiation, for example, fixes the peak power of the output pulse [3].

The addition of several amplifying stretches of fiber to the laser cavity makes it possible to effectively control the onset of the nonlinear phase of optical radiation in the laser cavity, allowing us to adjust the parameters of the output pulses over a wide range [3,4]. However, such approach complicates analysis of a constructed mode-locked laser.

The goal of this work was to implement a genetic algorithm to find the shortest pulse that is possible to generate inside figure-8 fiber laser cavity with two amplifying stretches of fiber.

The scheme of a figure-8 mode-locked fiber laser cavity is presented at Fig.1.a. Both loops of the laser resonator contain amplifying sections of 2.5 m long, which are pumped by independent multimode laser diodes with an optical power of up to 4 W at a wavelength of 978 nm. The right loop contains a high-power Faraday rotator, which provides unidirectional propagation of optical radiation. The loops are connected by a coupler 50/50. The output radiation is released from 70% port of the fiber coupler.

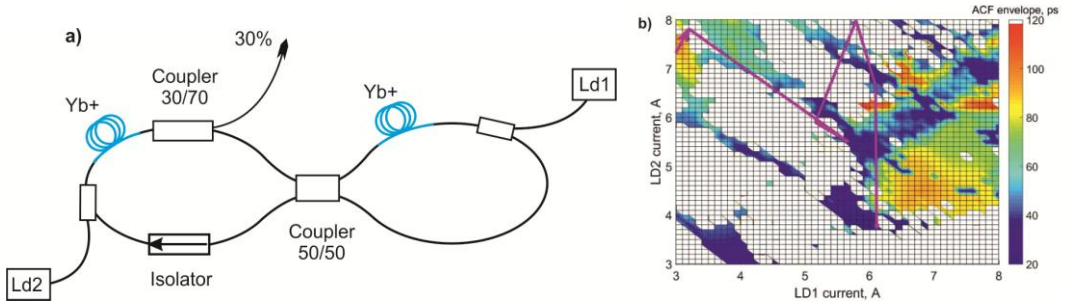

Fig. 1. a) Schematic of a fiber laser with two active stretches of fiber in both loops. b) Map of duration of the autocorrelation function of the output pulses

To overcome a problem with an adjustment of the pulse parameters we applied genetic algorithm that is based on the principle of artificial selection. The population consists of individuals with two genes each: the values of the currents of the pump diodes. Each individual is assigned a value of the fitness function that is a merit of the likeness to desired pulsed regime. Each step of the algorithm is a selection procedure that picks pulsed regime with a closest parameter to the desirable one. After each step of the algorithm genes of the part of individuals are mixed and randomly mutated. To prove the feasibility of the genetic algorithm we plotted the track of the best individual in population on the map of autocorrelation function Fig.1. b)

References

[1] M. Erkintalo, C. Aguergaray, A. Runge, and N. G. R. Broderick, "Environmentally stable all-PM all-fiber giant chirp oscillator," Opt. Express **20**, 22669 (2012).

[2] A. Ivanenko, S. Kobtsev, S. Smirnov, and A. Kemmer, "Mode-locked long fibre master oscillator with intra-cavity power management and pulse energy > 12 μJ," Opt.Express **24**, 6650 (2016).

[3] D. Li, L. Li, J. Zhou, L. Zhao, D. Tang, and D. Shen, "Characterization and compression of dissipative-soliton-resonance pulses in fiber lasers," Scientific Reports **6**, 23631 (2016).

[4] S.Smirnov, S.Kobtsev, A.Ivanenko, A.Kokhanovskiy, A.Kemmer, M.Gervaziev."Layout of NALM fiber laser with adjustable peak power of generated pulses," Optics Letters **42**, 1732 (2017).

[5] S. Kobtsev, A. Ivanenko, and A. Kokhanovskiy, "Electronic control of different generation regimes in mode-locked all-fibre F8 laser," Laser Physics Letters **15**, 045102 (2018).

Nonlinear Crystals for Photonics

K.E. Korzhneva [1,2], A.Yu. Tarasova[1,2*], A.A. Goloshumova[1,2], M.S. Molokeev[3], L.I. Isaenko[1,2]

[1]V.S. Sobolev Institute of Geology and Mineralogy SB RAS, Novosibirsk, Russia

[2]Novosibirsk State University, Novosibirsk, Russia

[3]Kirensky Institute of Physics SB RAS, Krasnoyarsk, Russia

**tarasovaau@igm.nsc.ru*

The need for new functional materials, single crystals of simple and complex compounds is continuously increasing in modern science and technology. However, their search and obtaining of crystals of large size, optical quality, stoichiometric composition are difficult. Non-centrosymmetric crystals of nitrates, carbonates and borates are promising for use in optoelectronics since they are transparent in the ultraviolet (UV) spectrum region and have a complex of nonlinear optical, piezoelectric and electro-optical properties [1, 2]. Systematic studies of the processes of crystallization of nitrates with complex composition, obtained from multicomponent solutions, are necessary both to clarify the principles of formation of perfect crystals and to obtain nonlinear materials.

The aim of present work is to investigate experimentally the processes of $K_2Ba(NO_3)_4$ and $Pb_{1-x}Ba_x(NO_3)_2$ double nitrates crystallization from aqueous solutions.

To obtain $K_2Ba(NO_3)_4$ double compound crystals from aqueous solutions several series of experiments were carried out in the temperature range of 72 – 30°C. The first series with the supersaturation of the solution with potassium nitrate, the second one with the supersaturation of barium nitrate with respect to the composition of the corresponding $K_2Ba(NO_3)_4$ stoichiometry. To obtain $Pb_{1,47}Ba_{0,53}(NO_3)_4$ crystals, $PbNO_3$ and $Ba(NO_3)_2$ were dissolved in water in a ratio of 4:1, experiments were carried out in the temperature range of 53 - 36°C. In the course of research $Pb_{1,47}Ba_{0,53}(NO_3)_4$ trigonal crystal and $K_2Ba(NO_3)_4$ tetragonal crystal were obtained.

The structures of $K_2Ba(NO_3)_4$ and $Pb_{1,47}Ba_{0,53}(NO_3)_4$ were decoded by x-ray diffraction analysis. The study revealed that $K_2Ba(NO_3)_4$ crystals have a tetragonal crystal structure with a lattice I -42m. The structure of $K_2Ba(NO_3)_4$ can be represented as the skeleton of BaO_{12} and KO_{12} polyhedra, linked together by oxygen ions belonging to the nitrate ions (Fig. 1). Crystals of $Pb_{1,47}Ba_{0,53}(NO_3)_4$ have a cubic crystal system with a lattice of Pa-3. The structure of $Pb/Ba/(NO_3)$ is similar to the structure of $K_2Ba(NO_3)_4$ and is a framework of vertex-linked Pb/Ba polyhedra, which have common edges with NO_3 triangles, and Pb and Ba take the same positions (Fig.1).

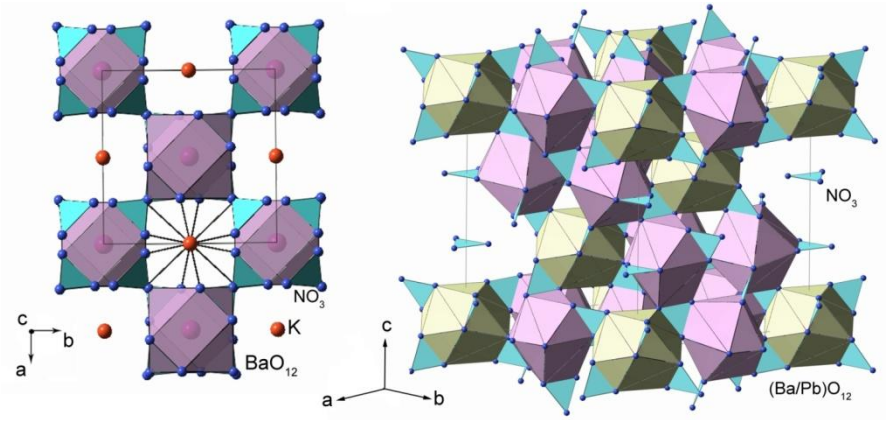

Fig. 1. Crystal structures of $K_2Ba(NO_3)_4$ (left) and $Pb_{1,47}Ba_{0,53}(NO_3)_4$ (right)

Using differential thermal analysis (DTA), it was found that $K_2Ba(NO_3)_4$ decomposes into $Ba(NO_3)_2$ and KNO_3 at 197°C, and this process is not reversible. $Pb_{1,47}Ba_{0,53}(NO_3)_4$ is stable up to 530°C. Raman spectra and transmission spectra for $K_2Ba(NO_3)_4$ and $Pb_{1,47}Ba_{0,53}(NO_3)_4$ crystals were obtained for the first time. It was found that Raman spectra of complex compounds differed from the spectra of simple nitrates. $K_2Ba(NO_3)_4$ crystals were found to be transparent in the range of 0.25-2.2 microns, but a strong absorption band with a maximum at about 0.3 microns was observed in the spectrum. The second harmonic generation of laser radiation with a wavelength of 1064 nm was observed for the obtained crystals, that confirmed their prospects for use in nonlinear optics.

The phase diagram of the KNO_3-$Ba(NO_3)_2$-H_2O triple system was constructed for the first time. Crystallization fields of simple nitrates and $K_2Ba(NO_3)_4$ double nitrate were selected.

The present work was supported by the Russian Foundation for Basic Research (grants №№ 18-32-00359, 17-45-540775).

References

[1] G. Shtukenberg, H. Euler, A. Kirfel, “Symmetry reduction and cation ordering in solid solutions of strontium-lead and barium-lead nitrates,” Z. Kristallogr. 221, 681 (2006).

[2] M.M. Markowitz, J.E. Ricci, P.F. Winternitz, “The system Ba(NO3)2-KNO3: Characterization of the Double Salt Ba(NO3)2*2KNO3,” J. Am. Chem. Soc. 77, 3482 (1995).

Nonlinear Optical Pulse Dynamics in a Bidirectional Ring Fibre Microcavity with Rayleigh Scattering and Intracavity Mirror

***V.A. Razukov*[1*], *L.A. Melnikov*[1]**
[1]*Yuri Gagarin State Technical University of Saratov, Saratov, Russia*
*razukov.vad@gmail.com

Nonlinear dynamics of the cavities and microcavities is a subject of extensive research, both experimental and numerical, because those cavities present effects that could be used in the widest range of science and industry applications. Examples of such effect include supercontinuum optical comb generations, optical gyro effects and et cetera [1].

In this work we continue to use the "CABARET" numerical method [2] to study the long time spatio-temporal dynamics of the electromagnetic field in a nonlinear ring fibre microcavity with dispersion over the hundreds and thousands of roundtrips. Our previous model of two ways propagating in opposite directions and mutually influencing each other [3,4], was expanded by introducing an intracavity mirror, Rayleigh scattering and nonreciprocal phase shift. We demonstrated forming of both temporal cavity solitons and irregular pulse trains.

The equations describing forward and backward wave propagation in the cavity are given as follows:

$$2i\left(\frac{\partial F}{\partial t}+v\frac{\partial F}{\partial z}\right)+D\frac{\partial^2 F}{\partial z^2}+2\chi\left(|F|^2+2|B|^2\right)F=0,$$
$$2i\left(\frac{\partial B}{\partial t}-v\frac{\partial B}{\partial z}\right)+D\frac{\partial^2 B}{\partial z^2}+2\chi\left(|F|^2+2|B|^2\right)B=0.$$

The boundary conditions are set like this:

$$F(0)=\sqrt{1-R}\sqrt{1-r}F(L)+\sqrt{R}\sqrt{A}\sqrt{1-r}+\sqrt{r}B(0),$$
$$B(L)=\sqrt{1-R}\sqrt{1-r}B(0)-\sqrt{r}(1-r)F(L)+\sqrt{Rr}\sqrt{1-R}\sqrt{A}.$$

Here F and B – field of the waves, propagating clockwise and counterclockwise respectively, $D>0$ – GVD coefficient, v – group velocity, χ – cross and self modulation coefficient, R – coupling unit reflection coefficient, r – intracavity mirror reflection coefficient, A – continuous pump intensity, L – cavity length. The figures below represent the calculation results for the two cavity configurations. The first case shows the results for a cavity with the relatively low (r=0,005) intracavity mirror reflection coefficient on the left, and relatively big on the right (r=0,05), Figure 1(a). The other case demonstrates the results with the Rayleigh scattering taken into the account. Low losses coefficient is on the left (lc=0,0001) and high losses coefficient is on the right (lc=0,001), Figure 1(b). Figure 2 displays the similar situation for the pulse shape on a single roundtrip along the cavity length with no Rayleigh scattering present, low intracavity mirror reflection coefficient on the left, large on the right, Figure 2(c), and Rayleigh scattering present, low losses on the left, large on the right, Figure 2(d).

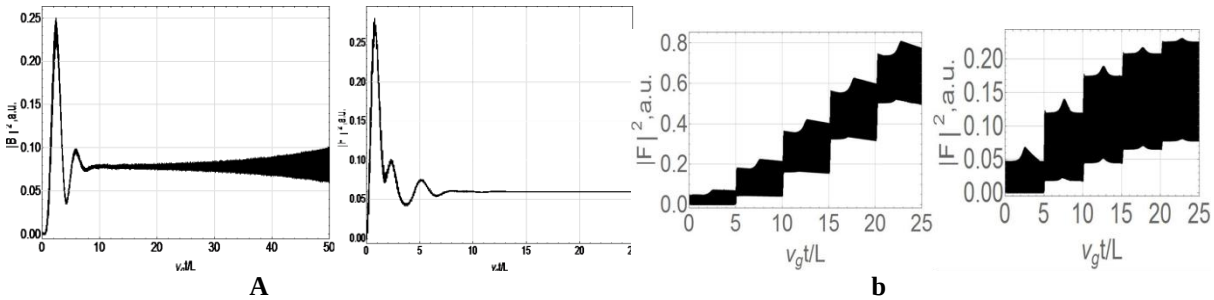

Fig. 1. Modeling results. Pulse energy versus the number of the cavity roundtrips

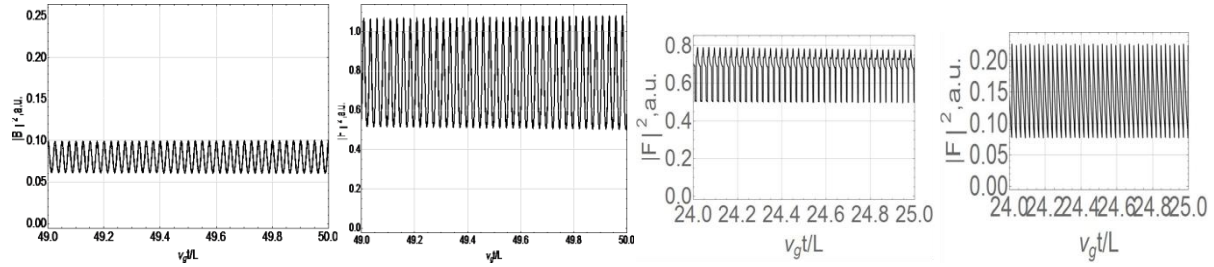

Fig. 2. Modeling results, pulse shape on a single roundtrip along the cavity length

Summarizing, we can conclude that in the case of no Rayleigh scattering present, there is either regime with a periodic pulse modulation on the cavity roundtrip, or a stationary regime, depending on the intracavity mirror reflection coefficient. Introduction of the Rayleigh scattering into the model leads to appearance of a very longtime transition process with discrete intensity gain occurring roughly every five roundtrips, what could be a trace of the longitudinal modes present inside of the cavity.

This work was supported by the Ministry of Science and Education of the Russian Federation, grant number 3.8493.2017/8.9.

References

[1] T. Herr, M. L. Gorodetsky, and T. J. Kippenberg in, *Nonlinear Optical Cavity Dynamics: From Microresonators to Fiber Lasers*, P. Grelu ed. (Wiley-VCH Verlag GmbH & Co. KGaA, Weinheim, Germany, 2016).

[2] V. M. Goloviznin, S. A. Karabasov, T. K. Kozubskaya, N. V. Maksimov, "CABARET scheme for the numerical solution of aeroacoustics problems: Generalization to linearized one-dimensional Euler equations," Computational Mathematics and Mathematical Physics, **49**, 2168 (2009).

[3] V. A. Razukov, L. A. Melnikov, "Short pulse dynamics in a linear cavity fiber laser," Proc. SPIE, **9917**, 9917-9917-5 (2016).

[4] V. A. Razukov, L. A. Melnikov, Yu. A. Mazhirina, S. V. Sukhanov, "Numerical modeling of space-temporal dynamics in fiber lasers," Journal of Applied Spectroscopy, **83**, 344 (2016).

Nonlinear Spectroscopy with Few-Cycle Pulses in Mid-Infrared: Mapping the Electron Band Structure by Intraband High-Harmonic Generation in Solids

E.A. Stepanov[1,2*], A.A. Lanin[1,2], A.B. Fedotov[1,2], A.M. Zheltikov[1,2,3]

[1]Physics Department, International Laser Center, M. V. Lomonosov Moscow State University, Vorob'evy gory, Moscow 119992, Russia

[2]Russian Quantum Center, 143025 Skolkovo, Moscow Region, Russia

[3]Department of Physics and Astronomy, Texas A&M University, 77843 College Station TX, USA

**ea.stepanov@physics.msu.ru*

High-order harmonic generation (HHG) in atomic gases is one of the key phenomena in strong-field laser–matter interactions, playing a central role in optical physics and rapidly growing attosecond technologies. When applied to solid materials [1 – 3], approaches of strong-field physics are subject to natural limitations, related to absorption and much lower laser damage thresholds of solids. As a reward, such solid-state extensions promise breakthroughs toward petahertz solid-state optoelectronics, open avenues toward attosecond science on the platform of solid-state materials, and suggest new all-optical methods for crystallographic analysis.

In presented work we study HHG in solids using mid-IR driver pulses within the wavelength range of 5.0 to 6.7 μm. In this wavelength region, a large group of below-the-bandgap high-order harmonics distinctly reflects, as our experiments show, an ultrafast dynamics of electron wave packets within the conduction and valence bands. We demonstrate that these harmonics directly relate to the nonlinearities of electron bands, providing a tool for electron band structure analysis in bulk solids. The intensities of individual optical harmonics as functions of the driver intensity I_0 were used to retrieve the energy dispersion profile for one of the electron conduction bands of ZnSe (Fig. 1) and to show that the result of this retrieval is consistent with the first-principle analysis of the electron band structure of ZnSe.

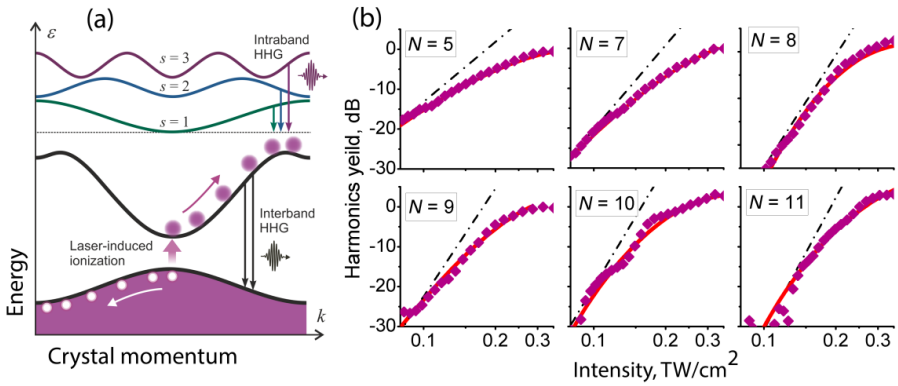

Fig. 1. (a) Inter and intraband HHG in a solid and electron band structure mapping. High-order harmonics are generated through the interband polarization involving electron-hole recombination, as well as through the modulation of the intraband current due to the nonlinearity of electron bands. (b) The power of the Nth-order optical harmonic generated by a 85- fs driver pulse with a central wavelength of 5.0 μm in a 2-mm-thick ZnSe film as a function of the driver intensity I_0. The dash-dotted lines show the I_0^N dependence. The solid lines present the best fit of the experimental data

Experimental work was performed with a frequency-tunable source of ultrashort mid-IR pulses [4, 5], which consists of two sequential stages of nonlinear-optical down conversion, involving optical parametric amplification in two cascaded BBO crystals, followed by difference-frequency generation in an AgGaS2 crystal. With pulse width of 85 fs, and energy ranging from 7 μJ at central wavelength $\lambda_0 \approx 5.0$ μm to 5 μJ at $\lambda_0 \approx 6.7$ μm, the output radiation was focused by a 15x, 0.30-NA reflective objective onto a ZnSe sample, delivering field intensities up to 4 TW/cm^2.

This work was supported by the Russian Foundation for Basic Research (16-32-60163, 16-29-11799, 18-32-00782) and Foundation for the advancement of theoretical physics “BASIS”.

References

[1] S. Ghimire, A. D. DiChiara, E. Sistrunk, P. Agostini, L. F. DiMauro, and D.A. Reis, "Observation of high-order harmonic generation in a bulk crystal," Nature Phys. 7, 138 (2011).

[2] G. Vampa, T. J. Hammong, N. Thiré, B. E. Schmidt, F. Légaré, C. R. McDonald, T. Brabec, and P. B. Corkum, "Linking high harmonics from gases and solids," Nature 25, 462 (2015).

[3] M. Hohenleutner, F. Langer, O. Schubert, M. Knorr, U. Huttner, S. W. Koch, M. Kira, and R. Huber, “Real-time observation of interfering crystal electrons in high-harmonic generation,” Nature 523, 572 (2015).

[4] E. A. Stepanov, A. A. Lanin, A. A. Voronin, A. B. Fedotov, and A. M. Zheltikov, "Solid-State Source of Subcycle Pulses in the Midinfrared," Phys. Rev. Lett. 117, 043901 (2016).

[5] A. A. Lanin, A. A. Voronin, E. A. Stepanov, A. B. Fedotov, and A.M. Zheltikov, "Multioctave, 3–18 μm sub-two-cycle supercontinua from self-compressing, self-focusing soliton transients in a solid," Opt. Lett. 40, 974 (2015).

Analysis of Aberrations in Heterodyne Time Microscope

A. Tikan, S. Bielawski, C. Szwaj, S. Randoux, P. Suret*
Laboratoire de Physique des Lasers, Atomes et Molecules, UMR-CNRS 8523,
Université de Lille, Villeneuve-d'Ascq, France
Centre d'Etudes et de Recherches Lasers et Applications (CERLA), Villeneuve-d'Ascq, France
**pierre.suret@univ-lille1.fr*

The "world" of nonlinear photonics is growing every year. More and more complex and subtle phenomena are getting into the area of interest. Many of effects in this domain can be observed only on very short time scales (picoseconds and less). This fact unavoidably poses a problem of measurements of these ultrafast events. Some of them (for example stochastic phenomena) requires measurements in single-shot with sub-picosecond resolution over a window of tens of picoseconds and a wide dynamic range.

The field of ultrafast measurements demonstrated significant progress in the last 30 years, but the problem of construction of the full optical oscilloscope, which is able to measure simultaneously the phase and intensity at single-shot, was solved just recently [1-3]. Both solutions presented in the review are based on the temporal imaging approach [4-6]. Temporal imaging is a technique built on the analogy between paraxial diffraction in space and dispersion in time. However, this approach suffers from aberrations similar to ones in classical optics [7].

Here we present a study of the resolution limitations of Heterodyne Time Microscope (HTM) and its modified version Spatial Encoding Arrangement with Hologram Observation for Recording in Single-shot the Electric field (SEAHORSE) [2]. We report that the HTM provides direct simultaneous intensity and phase measurements over a window of 40 ps with 250 fs resolution. We demonstrate a crucial role of the aberrations in recoding of ultrafast signals. The SEAHORSE was built in order to decrease the aberrations using the method of digital holography [6]. With the SEAHORSE we recorded temporal holograms allowed to obtain 70 fs resolution, keeping the same window of measurements as in the case of HTM.

References

[1] C. Lei, K. Goda, "The complete optical oscilloscope," Nat. Photon. 12, 190 (2018).

[2] A. Tikan, S. Bielawski, C. Szwaj, S. Randoux, P. Suret, "Single-shot measurement of phase and amplitude by using a heterodyne time-lens system and ultrafast digital time-holography," Nat. Photon., 12, 228 (2018).

[3] P. Ryczkowski, et al. "Real-time full-field characterization of transient dissipative soliton dynamics in a mode-locked laser," Nat. Photon., 12, 221 (2018).

[4] P. Suret, et al. "Single-shot observation of optical rogue waves in integrable turbulence using time microscopy," Nat. Commun.,7, 13136 (2016).

[5] M. Närhi, et al. "Real-time measurements of spontaneous breathers and rogue wave events in optical fibre modulation instability," Nat. Commun., 7, 13675 (2016).

[6] B. H. Kolner, M. Nazarathy, "Temporal imaging with a time lens," Opt. Lett. 14, 630 (1989).

[7] C. V. Bennett, B. H. Kolner, "Aberrations in temporal imaging," IEEE J. Quantum Electron. 37, 20 (2001).

[8] U. Schnars, W. Jüptner, *Digital holography*, (Springer, Berlin, Heidelberg, 2005).

Precision Spectroscopy of Cold Magnesium Atoms for an Optical Frequency Standard

M.A. Tropnikov[1*], A.E. Bonert[1], A.N. Goncharov[1,2,3], S.N. Kuznetsov[1], V.I. Baraulya[1], D.V. Brazhnikov[1,2], O.N. Prudnikov[1]

[1]Institute of Laser Physics of the Siberian Branch of the Russian Academy of Sciences, Novosibirsk, Russia

[2]Novosibirsk State University, Novosibirsk, Russia

[3]Novosibirsk State Technical University, Novosibirsk, Russia

makstropnikov@gmail.com

Frequency standards play an important role in various fields of science and technology. The relative accuracy of a primary frequency standard based on a caesium fountain has probably reached its limit $\Delta\nu/\nu = 2*10^{-16}$ [1]. Further increase in the accuracy of frequency standards is associated with the creation of optical frequency standards based on single ions or neutral atoms. Alkaline-earth and alkaline-earth-like atoms, such as Yb, Ca, Sr, Hg, and Mg, are among the main candidates for creating the optical frequency standards. The most accurate and stable optical frequency standards for today are optical frequency standards based on Sr and Yb atoms captured in the optical lattice. ^{24}Mg has some advantages over the other candidates such as the narrowest intercombination transition, the simplest structure of the electron shells, and the smallest frequency shift of the "clock" transition due to black body radiation. The presence of strong closed $^1S_0$–$^1P_1$ transition allows effective cooling and trapping of magnesium atoms in a magneto-optical trap. Creation of a frequency standard based on Mg atoms is possible using $^1S_0$–$^3P_1$ transition with the natural linewidth of 36 Hz. In this paper, the possibility of obtaining the narrow reference lines using $^1S_0$–$^3P_1$ transition in creating the optical frequency standard is shown and the progress achieved in the frequency stabilization by observed resonances studies is presented.

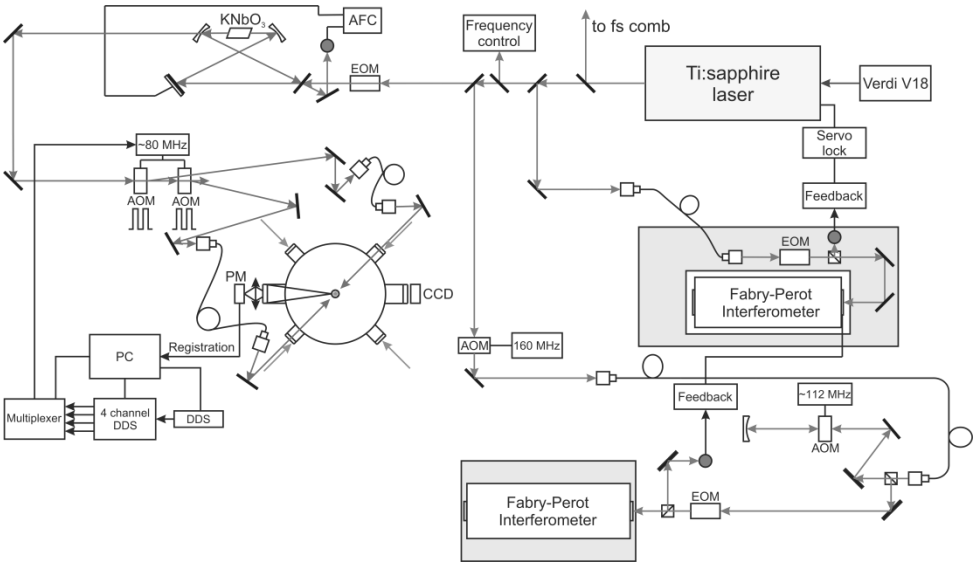

Fig. 1. Schematic of the experimental setup used for spectroscopy of the clock transition. Fs comb – femtosecond comb, $KNbO_3$ – nonlinear crystal in an external cavity, AFC – automatic frequency control, AOM – acousto-optic modulator, EOM – electro-optic modulator, DDS – 4-channel direct digital synthesizer, PM – photomultiplier tube, CCD – CCD camera

The source of radiation for clock $^1S_0$–$^3P_1$ transition spectroscopy is a system based on Ti:sapphire laser pumped by 15-watt solid-state Verdi V18 laser with a two-stage system of

frequency stabilization and a frequency doubling in a $KNbO_3$ crystal in an external cavity. The stabilized Ti:sapphire laser outputs about 1 W of power at 914 nm and cavity enhanced second harmonic generation inside a nonlinear $KNbO_3$ crystal yields about 80 mW at 457 nm. Laser cooling and localization of magnesium atoms in a magneto-optical trap is carried out on the $^1S_0$–$^1P_1$ closed transition at 285 nm.

Investigation of the $^1S_0$–$^3P_1$ transition of cold magnesium atoms localized in the MOT is performed by the method of fields separated in time. Two pairs of the light pulses formed from cw radiation of a highly stable laser system at 457 nm by acousto-optic modulators interact with a cloud of magnesium atoms. In recording narrow resonances, the radiation frequency of the laser system is tuned by a frequency synthesizer controlling AOM in the second stabilization system. The pulse duration τ is 4 μs and the time delay T for a pair of unidirectional pulses could be varied to achieve needed spectral resolution $\Delta\nu = 1/(8T_{eff})$, where $T_{eff} = (4/\pi)\tau + T$. The best to date spectral resolution is $\Delta\nu = 390$ Hz (Fig. 2(a)).

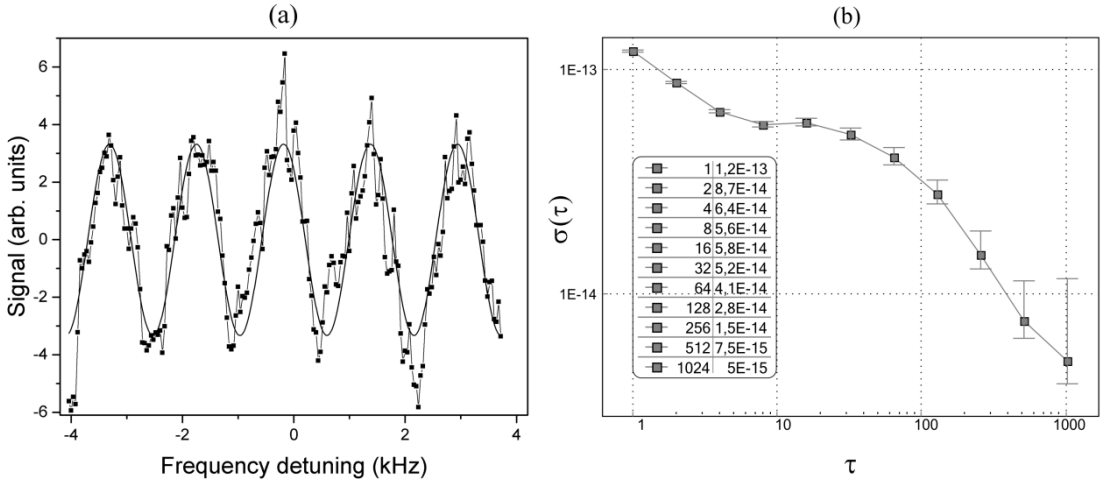

Fig. 2. (a) Resonances in time-separated fields for the delays between pulses T=310 μs. (b) Allan function characterizing frequency stability of the developed Mg frequency standard

The error signal for stabilizing the clock laser frequency by the central fringe of observed resonances is formed using a digital analogue of stabilisation with respect to the third harmonic of the modulation frequency [2]. The calculated value was used to tune the AOM frequency in the second stabilization system. To determine the frequency stability for the radiation stabilized, some part of clock laser radiation at a wavelength of 914 nm was directed through an optical fiber to a stabilized femtosecond frequency comb, based on a Ti:sapphire laser. Fig. 2(b) shows the measured frequency stability of $5 \cdot 10^{-15}$ at averaging time $\tau = 1000$ s.

References

[1] F. Levi, D. Calonico, C. E. Calosso, A. Godone, S. Micalizio, and G. A. Costanzo. “Accuracy evaluation of ITCsF2: a nitrogen cooled caesium fountain", Metrologia, **51(3)**, 270 (2014).

[2] C. Degenhardt, H. Stoehr, C. Lisdat, G. Wilpers, H. Schnatz, B. Lipphardt, T. Nazarova, P. Pottie, U. Sterr, J. Helmcke, and F. Riehle. “Calcium optical frequency standard with ultracold atoms: Approaching 10−15 relative uncertainty”, Phys. Rev. A. **72(6)**, 062111 (2005).

Investigation of Various Pulsed Regimes of Generation of an Erbium Fiber Laser with a Resonator Length of more than 200 m

I.A. Volkov[1*], S.N. Ushakov[1,2], K.N. Nishchev[1], V.A. Kamynin[2], V.V. Tsvetkov[2]
[1]National Research Mordovia State University, Saransk, Russia
[2]A.M. Prokhorov General Physics Institute of the Russian Academy of Sciences, Moscow, Russia
emofan_80@mail.ru

Pulsed fiber lasers have found many new applications in such areas as laser science, optical communications, biomedical research and industrial technology. To date, the most widely used means of amplification for fiber lasers are fibers doped with Er^{3+} and Yb^{3+} ions. In modern fiber lasers, various mechanisms of passive mode-locking are used. One of these is the use of the Kerr nonlinearity of optical fibers to achieve a nonlinear evolution of the polarization in a laser cavity [1, 2]. This mechanism of mode-locking makes it possible to realize fiber lasers without precision optomechanical elements.

In this work, we realized and investigated EDFA capable of discrete pulse width adjustment. Various modes of laser operation, including fundamental mode-locking and soliton mode, are obtained by adjusting the intracavity polarization controller.

In Fig. 1 a ring laser circuit is presented. Pumping was carried out through a fiber power combiner with a laser multimode diode with an output power of up to 4 W with a wavelength of 970 nm. The pump diode power is set at 1.28 W. The laser resonator is formed by a single-mode fiber SM-E3 and a fiber doped with erbium. The length of the active fiber SM-EYDF-6/125-HE was 3 m, and the length of the entire resonator was 215 m. The direction of generation in the circuit was determined by the fiber isolator. Two 3-paddle polarization controllers are installed in the ring resonator on both sides of the fiber polarization divider and are used to adjust the polarization.

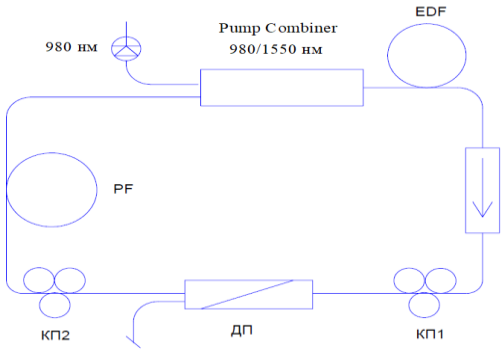

Fig.1. Experimental setup of the ring-cavity EDF laser. EDF - fiber doped with Yb/Er ions; PF is a passive fiber; DP (ДП) is a polarization divisor; CP (КП)1,2 - controllers of polarization 1,2

The output of the laser is connected by means of an optical socket to the 1/3 splitter, which allows controlling the output characteristic of the laser. The emission spectra were obtained using an optical spectrum analyzer Yokogawa AQ6370C with a resolution of 0.2 nm, for oscillograms of pulses - oscillographs GWINSTEK GDS-3000 (500MHz) and Tektronix MSO 5204 (2GHz) with high-speed radiation receiver based on InGaAs PIN photodiode. To measure the width of pulses with passive synchronization, a scanning autocorrelator AA-20M was used.

In Fig. 2. the spectra and oscillograms of the pulses for the regimes obtained are presented, as well as the autocorrelation function for fundamental mode-locking.

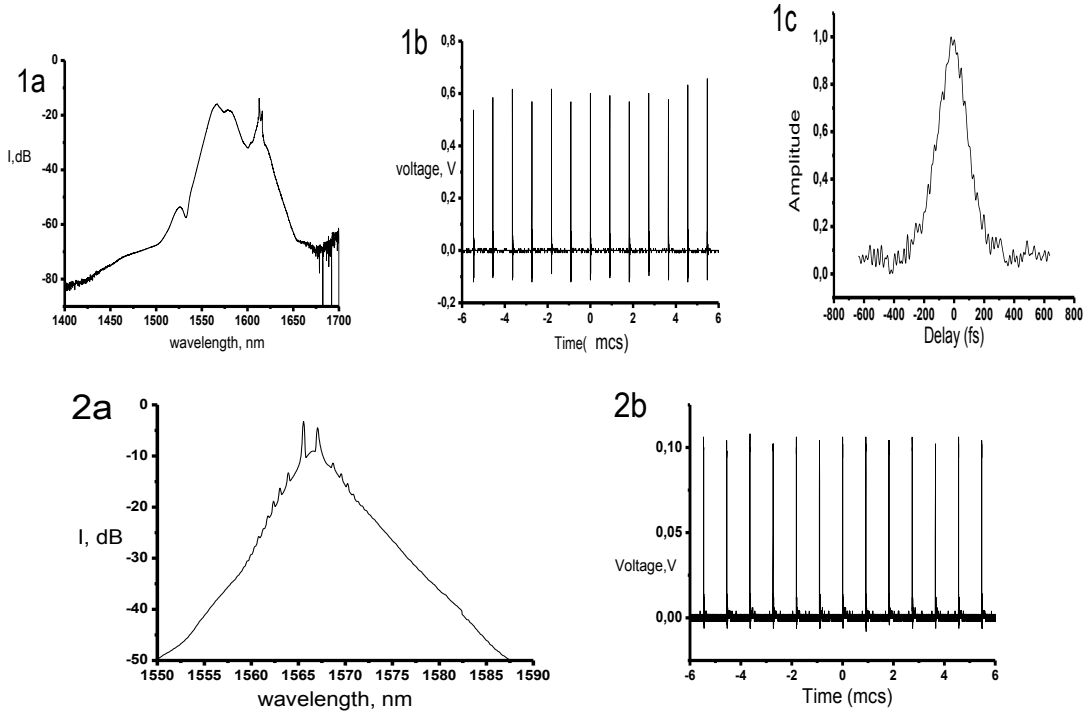

Fig. 2. 1 - fundamental mode-locking.: a) spectrum; b) an oscillogram; c) ACF.
2 - soliton regime: a) spectrum; b) an oscillogram

The pulse repetition rate for the regimes was 1.09 MHz. The spectrum in mode 1 is deformed with an explicit Raman shift. The central wavelength was 1570 nm, with a spectral width of 17.85 nm. From the ACF data, the duration in this regime was 165fs. At the output of the mode 2 spectrum, Kelly's sideband is visible, which are characteristic for the soliton regime. In this regime, the spectrum width at the 3dB level was 2.5 nm at a central wavelength of 1566.5 nm. From the spectrum for the soliton regime, the duration was determined $\tau = \frac{K*\lambda_c^2}{c*\Delta\lambda} = 1{,}03ps$, and taking into account the Cadel formula [3], the intracavity dispersion $\beta_2 L \approx 3$ ps^2.

References

[1] W.-H. Kuan et al. “Femto/nano-second switchable passively mode-locked fiber laser with analytic modeling by the cubic-quintic Ginzburg-Landau equation,” Optics Letters, **43** (2018).

[2] J. Liu et al. “Generation and evolution of mode-locked noiselike square-wave pulses in a large-anomalousdispersion Er-doped ring fiber laser,” Optics Express, **23**, (2015).

[3] R. Kadel, B. R. Washburn “All-fiber passively mode-locked thulium/holmium laser with two center wavelengths,” Applied Optics, **51** (2012).

High Power Passively Mode-Locked Thulium-Doped All-Fiber Ring Laser for Supercontinuum Generation in Mid-IR

V.S. Voropaev[1], A.I. Donodin[1], A.I. Voronets[1], V.A. Lazarev[1], M.K. Tarabrin[1,2], V.E. Karasik[1] and A.A. Krylov[3]

[1] Science and Education Center for Photonics and IR-Technology, Bauman Moscow State Technical University, Moscow, Russia, 105005

[2]P.N. Lebedev Physical Institute of the Russian Academy of Sciences, Moscow, Russia

[3]Fiber Optics Research Center of the Russian Academy of Sciences, Moscow, Russia, 119333

vasilii.s.voropaev@gmail.com

The mid-IR spectroscopy is an interesting field for science, technology and medicine, since a large number of molecules have rotational absorption lines in this range [1]. The use of broadband laser frequency combs instead of thermal light sources (globar, tungsten lamp) in the mid-IR range can significantly improve the sensitivity of spectroscopic methods [2], which will allow devices for detecting small traces of environmental and toxic gases up to the sensitivity of parts per billion in various applications. For example, in medicine, the detection of small concentrations of certain molecules in exhaled air can be used to diagnose human diseases [3].

A broadband spectrum of laser radiation in the mid-IR range can be obtained by a supercontinuum generation in highly nonlinear fibers pumped by ultrashort pulses. Femtosecond thulium-doped fiber laser systems are compact, easy to align, reliable and have demonstrated the generation of a wide supercontinuum in special highly nonlinear fibers in the wavelength range from 1 to 9 μm [4,5]. In this paper, we demonstrate the generation of high-energy ultrashort pulses at a wavelength of 1890 nm with a pulse repetition rate of 13 MHz, with an average power of 560 mW and pulse energy of 43 nJ directly in passively mode-locked thulium-doped all-fiber ring laser for a supercontinuum generation in highly nonlinear mid-IR fibers.

The all-fiber ring laser cavity (fig.1a) [6] consisted of three fiber types: SMF-28, SMF-LS, active thulium-doped fiber. All fibers had a negative dispersion (fig.1b). The total cavity dispersion was equal -0.85 ps^2. The active fiber was pumped by an Er/Yb fiber laser at a wavelength of 1550 nm with a maximum power of 2.6 W through the fiber fused wavelength-division multiplexer (WDM 1550/2000 nm). The nonlinear polarization evolution as mode-locking mechanism was realized using two polarization controllers (PC) and an isolator-polarizer. To achieve a higher generation efficiency, the output connector extracted 72% radiation from the cavity. With different settings of the polarization controllers in the laser, two generation regimes differing in the width of the spectrum and in the duration of the pulses were observed. For both generation regimes, optical spectra, intensity autocorrelation and generation efficiency are shown in Figure 2.

To best of our knowledge [7], the highest pulse energy and average power ever generated directly in passively mode-locked Tm-doped all-fiber lasers were obtained in this work. At present, we are studying the supercontinuum generation in different mid-IR fibers pumped by a developed laser.

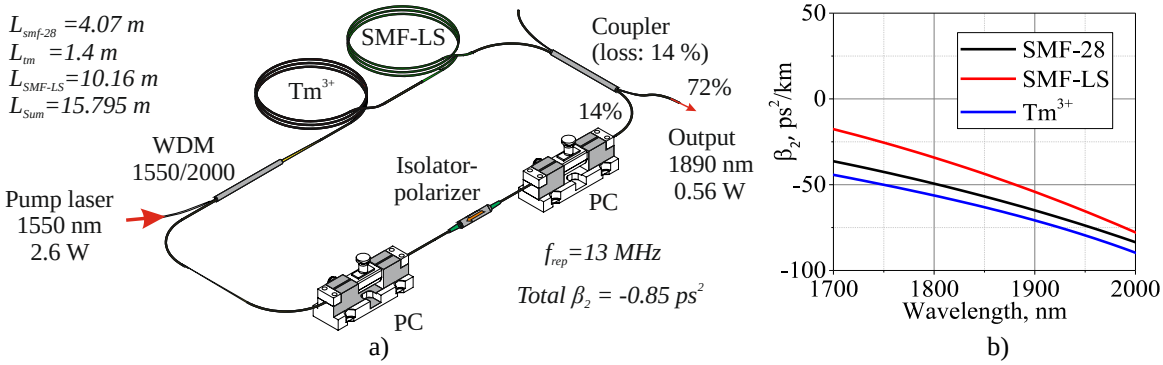

Fig. 1. Laser schematic and characteristics: a) Tm-doped fiber laser setup; b) Group velocity dispersion of the laser cavity fibers

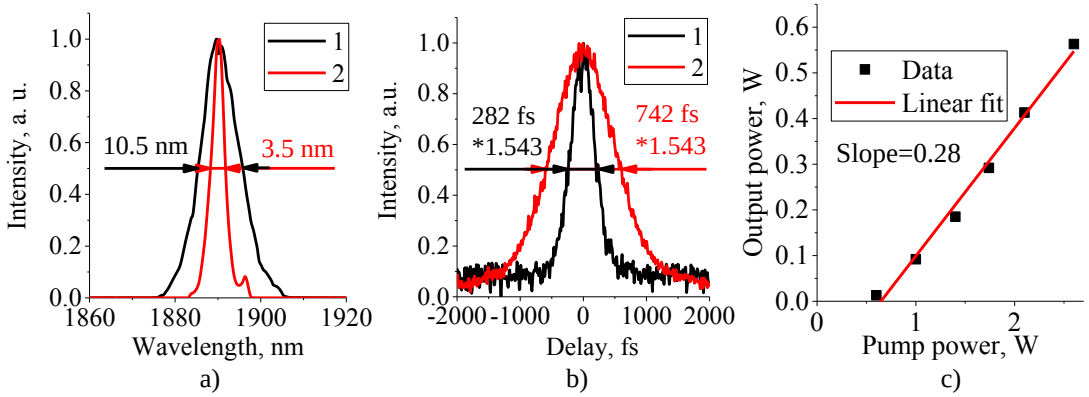

Fig. 2. Characteristics of two generation regimes: spectrum (a), intensity autocorrelation traces (b), Laser average output power versus pump power in mode-locked regime (c)

References

[1] A. Schliesser, N. Picqué and T. W. Hänsch, "Mid-infrared frequency combs," Nat. Photonics. **6**, 440 (2012).

[2] C. R. Petersen et al., "Mid-infrared supercontinuum covering the 1.4–13.3 μm molecular fingerprint region using ultra-high NA chalcogenide step-index fibre," Nat. Photonics. **8**, 830 (2014).

[3] Z. Bielecki et al. "Selected optoelectronic sensors in medical applications," Opto-electron. Rev. **26**, 122 (2018).

[4] I. Kubat et al., "Thulium pumped mid-infrared 0.9-9μm supercontinuum generation in concatenated fluoride and chalcogenide glass fibers," Opt. Express. **22**, 3959 (2014).

[5] R. Salem et al., "Mid-infrared supercontinuum generation spanning 1.8 octaves using step-index indium fluoride fiber pumped by a femtosecond fiber laser near 2 μm," Opt. Express. **23**, 30592 (2015).

[6] V. Voropaev et al., " All-fiber passively mode-locked ring laser based on normal dispersion active Tm-doped fiber," in Frontiers in Optics 2017, paper JTu3A.15. (2017).

[7] M. A. Chernysheva et al.**,** "Higher-Order Soliton Generation in Hybrid Mode-Locked Thulium-doped Fiber Ring Laser," IEEE J. Sel. Top. Quantum Electron. **20**, 425 (2014).

Octagonal-Core Anti-Resonant Hollow-Core Fiber for Near-IR Spectral Range

E.A. Yelistratova[1,*], V.V. Demidov[2], V.A. Ananyev[2,3], G.K. Alagashev[4], S.O. Leonov[1]
[1] Bauman Moscow State Technical University, Moscow, Russia
[2] Research and Technological Institute of Optical Materials All-Russia Scientific Center "S.I. Vavilov State Optical Institute", St. Petersburg, Russia
[3] Department of Optical Information Technologies and Materials at the Saint Petersburg National Research University of Information Technologies, Mechanics and Optics, St. Petersburg, Russia
[4]Fiber Optics Research Center, Russian Academy of Sciences, Moscow, Russia
**thesamelisa@gmail.com*

Recent progress in hollow-core photonic bandgap fibers (HC-FBGFs) has given new possibilities in nonlinear optics of laser-matter interaction [1] and low-loss mid-infrared transmission [2]. The hollow-core of this fibers can be filled with appropriate gases or liquids [3], leading to long interaction length between light and matter. In this case, strong nonlinear effects could be achieved by the confinement of light in a small mode area and to the extremely long interaction lengths [4]. Several types of HC-FBGFs were used to obtain nonlinear interaction in gases, for example, original HC-FBGFs with a full two-dimensional photonic bandgap, Kagome lattice hollow-core fibers (HCFs) and negative curvature HCFs, which anti-resonant properties depend strongly on the core size and the shape of the core-cladding boundary [5].

In this paper we report on hollow octagonal-core fiber, its transmission spectrum, optical losses and mode properties.

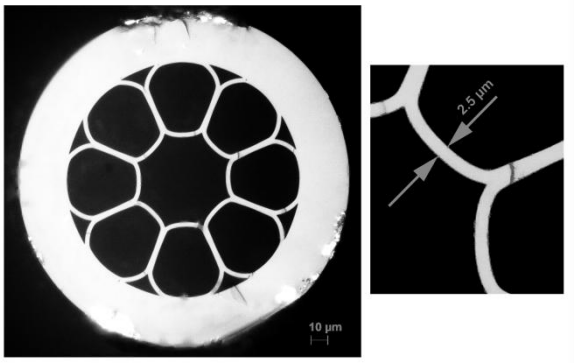

Fig. 1. Profile of the hollow octagonal-core fiber (left) and enlarged image of the core-cladding boundary layer (right)

The fiber geometry is shown on figure 1. HCF was fabricated using the conventional stack-and-draw technique. The fiber was designed as eight touching capillaries providing the octagonal shape of the core and characterized by the core diameter of 50 μm, outer diameter of 198 μm and the wall thickness at the core-cladding boundary of 2.5 μm. The small negative curvature of the core-cladding boundary was obtained by putting an excessive gas pressure inside capillaries during the drawing process.

The optical losses were calculated using FEM simulation (Fig. 2). The transmission spectrum of the fiber was measured with broadband source and optical spectrometer. As it can be seen in Fig. 2 the observed HCF has transmission windows near wavelengths of 1250 nm, 1650 nm, and 2200 nm. The calculated optical losses for these transmission windows range from 20 to 5 dB/m. We also measured losses and output mode profiles at 1250 nm and 1650 nm. The results are shown by green circles in Fig. 2 and are 15 dB/m for 1250 nm and 8 dB/m for 1650 nm.

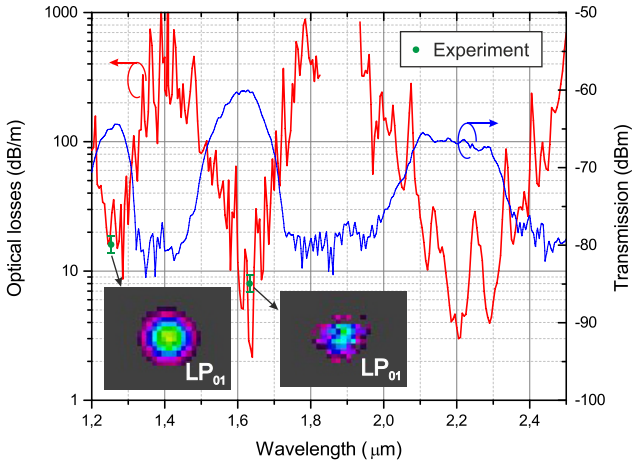

Fig. 2. Calculated optical losses and measured transmission spectrum for HCF in the near-IR spectral range. Insets: far-field mode profile at 1250 nm and 1650 nm

In summary, silica-based anti-resonant hollow octagonal-core fiber with the core diameter of 50 μm was designed and implemented. The HCF performs well in the near-IR spectral range with losses vary from 5 to 20 dB/m. In the observed spectral ranges single-mode transmission was achieved.

The reported study was funded by RFBR, according to the research project No. 17-08-00495.

References

[1] P. S. J. Russell, P. Holzer, W. Chang, A. Abdolvand, and J. C. Travers, "Hollow-core photonic crystal fibers for gas-based nonlinear optics," Nature Photonics **8,** 278, (2014).

[2] F. Yu, W. J. Wadsworth and J. C. Knight, "Low loss silica hollow core fibers for 3–4 μm spectral region," Opt. Express **20,** 11153, (2012).

[3] A. R. Bhagwat and A. L. Gaeta, "Nonlinear optics in hollow-core photonic bandgap fibers," Opt. Express **16**, 5035, (2008).

[4] F. Poletti, M. N. Petrovich, and D. J. Richardson, "Hollow-core photonic bandgap fibers: technology and applications," Nanophotonics **2**, 315-340, (2013).

[5] A. D. Pryamikov, G. K. Alagashev, A. F. Kosolapov and A. S. Biriukov, "Impact of core-cladding boundary shape on the waveguide properties of hollow core microstructured fibers," Laser Physics **26,** 125104 (2016).

[6] N. M. Litchinitser, A. K. Abeeluck, C. Headley, and B. J. Eggleton, "Antiresonant reflecting photonic crystal optical waveguides," Opt. Lett. **27**, 1592, (2002).

All-Fiber Erbium Mode-Locked Hybrid Laser with High Energy Pulses

***I.S. Zhdanov*[1,2], *D.S. Kharenko*[1,2], *S.A. Babin*[1,2]**
[1]*Institute of Automation and Electrometry SB RAS, Novosibirsk, Russia*
[2]*Novosibirsk State University, Novosibirsk, Russia*
*inn.zhdanov@rambler.ru

Ultrafast lasers with a high pulse energy at 1550-nm carrier wavelength attract high attention for last years and have a wide spectrum of applications: CARS [1], few-cycle pulse generation [2], frequency metrology [3,4], and THz radiation generation [5]. All of these applications require a high pulse peak power, short duration, and high generation stability.

Highly chirped (chirp parameter > 10) dissipative soliton (HCDS) generation regime satisfies the described requirements. A quite significant HCDS energy increase have been obtained in the all-fiber Ytterbium NPE mode-locked cavity consisting of polarization maintaining (PM) and non-PM parts [6]. We have realized this approach for 1.5 microns wavelength region for the first time [7]. The generated pulses from the erbium all-fiber hybrid cavity had 165 fs dechirped duration and 0.93 nJ energy. This work aims to increase the HCDS energy generated directly from the master oscillator.

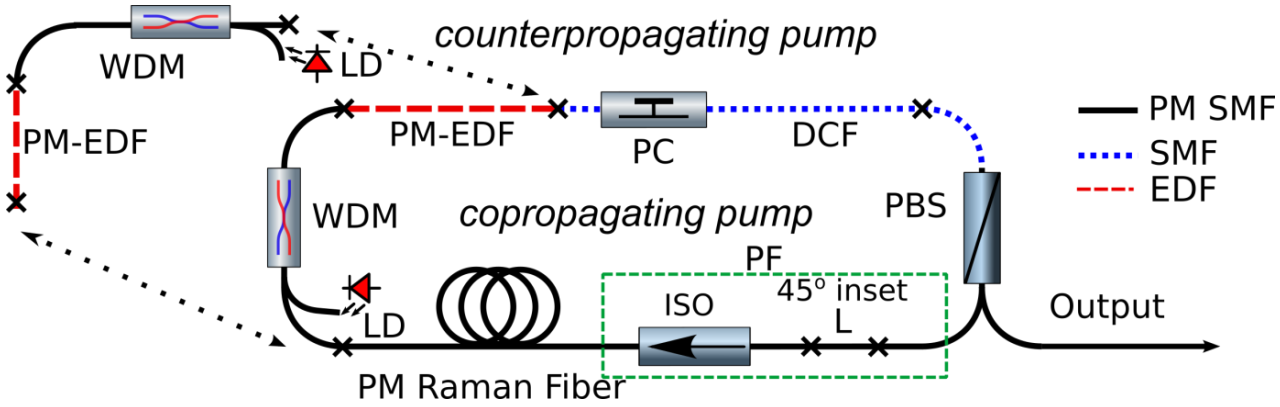

Fig. 1. The scheme of the experimental setup in a copropaganting and counterpropagating pump configuration: ***PM SMF*** *– polarization maintaining single mode fiber,* ***SMF-*** *single mode fiber,* ***EDF*** *– Erbium-doped fiber,* ***WDM*** *– wavelength division multiplexer,* ***DCF*** *– dispersion compensated fiber,* ***PBS*** *– polarization beam splitter,* ***LD*** *– laser diode,* ***PF –*** *polarization filter,* ***ISO*** *– optical fiber isolator*

The energy increase was realized by the lengthening of the cavity with a PM-fiber section. For this purpose we used several types of fiber (Fujikura DS-15, PM 1550-XP, OFS PM Raman), but most of them had anomalous dispersion at 1550 nm that negatively affected the net cavity dispersion. As a result PM Raman fiber (OFS) was used because of its high normal dispersion. Two cavity configurations were tested with a copropagating and a counterpropagating pump correspondingly (Fig. 1). Copropagating pump scheme is able to generate HCDS pulses with 3.3-3.7 nJ energy, Fig. 2a depicts the spectra for 35 nm filter laser. In the counterpropagating configuration the pulse energy increased up to 5.1-5.9 nJ. However, the spectrum of the generated pulses became smooth and wide (Fig. 2b). It is noted the Raman radiation was not observed. During the presentation optical spectra, RF spectra, and interferometric autocorrelation of the generated pulses will be presented.

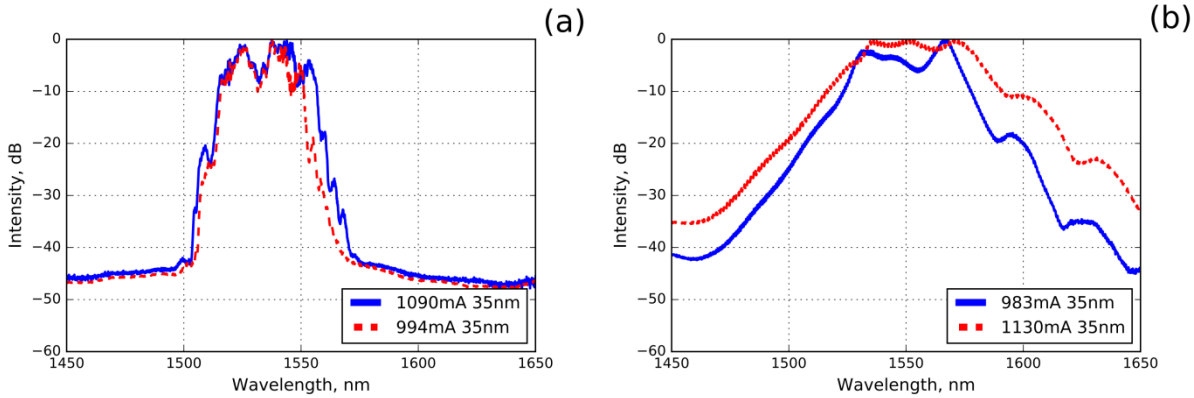

Fig. 2. Spectra of the generated pulses in a copropagating pump scheme **(a)** and counterpropagating pump configuration **(b)**

References

[1] C. W. Freudinger, W. Yang, G. R. Holtom, N. Peyghambarian, X. S. Xie, K. Q. Kieu, "Stimulated Raman scattering microscopy with a robust fibre laser source," Nat. Photonics **8**, 153 (2014).

[2] G. Krauss, S. Lohss, T. Hanke, A. Sell, S. Eggert, R. Hubler, A. Leitenstorfer, "Synthesis of a single cycle of light with compact erbium-doped fibre technology," Nat. Photonics **4**, 33 (2010).

[3] V. S. Pivtsov, B. N. Nyushkov, I. I. Korel, N. A. Koliada, S. A. Farnosov, V. I. Denisov, "Development of a prototype compact fibre frequency synthesiser for mobile femtosecond optical clocks," Quantum Electronics, **44**, 06 (2014).

[4] N. R. Newbury, W. C. Swann, "Low-noise fiber-laser frequency combs," J. Opt. Soc. Am. B, **24,** 1756 (2007).

[5] A. Schneider, M. Stillhart, and P. Günter, "High efficiency generation and detection of terahertz pulses using laser pulses at telecommunication wavelengths," Opt. Express **14**, 5376 (2006).

[6] D. S. Kharenko, E. V. Podivilov, A. A. Apolonski, and S. A. Babin, "20 nJ 200 fs all-fiber highly chirped dissipative soliton oscillator," Opt. Lett. **37**, 4104 (2012).

[7] D. S. Kharenko, I. S. Zhdanov, A. E. Bednyakova, E. V. Podivilov, M. P. Fedoruk, A. A. Apolonski, S. K. Turitsyn, and S. A. Babin, "All-fiber highly chirped dissipative soliton generation in the telecom range," Opt. Letters **42**, 3221 (2017).